On the Water−Carbon Interaction for Use in Molecular Dynamics Simulations of Graphite and Carbon Nanotubes

T. Werder,*,† J. H. Walther,† R. L. Jaffe,‡ T. Halicioglu,§ and P. Koumoutsakos†,‖

Institute of Computational Science, ETH Zürich, CH-8092 Zürich, Switzerland, NASA Ames Research Center, Moffett Field, California 94035, and Eloret Corporation, 690 West Fremont Avenue, Sunnyvale, California 94086

A systematic molecular dynamics study shows that the contact angle of a water droplet on graphite changes significantly as a function of the water−carbon interaction energy. Together with the observation that a linear relationship can be established between the contact angle and the water monomer binding energy on graphite, a new route to calibrate interaction potential parameters is presented. Through a variation of the droplet size in the range from 1000 to 17 500 water molecules, we determine the line tension to be positive and on the order of 2×10^{-10} J/m. To recover a macroscopic contact angle of 86°, a water monomer binding energy of -6.33 kJ mol^{-1} is required, which is obtained by applying a carbon−oxygen Lennard-Jones potential with the parameters $\epsilon_{CO} = 0.392$ kJ mol^{-1} and $\sigma_{CO} = 3.19$ Å. For this new water−carbon interaction potential, we present density profiles and hydrogen bond distributions for a water droplet on graphite.

1. Introduction

The possibility of functionalizing carbon nanotubes (CNT), their high mechanical strength, and their unusual electronic properties make possible a broad range of innovative applications for CNTs in sensor technology. The first successful sensor implementations based on CNTs include electromechanical,[1] chemical,[2] and biological sensors.[3,4] Because biosensors usually operate in aqueous environments, it is important to have a thorough understanding of the interaction between CNTs and water. The wetting properties of single-wall CNTs, which are determined by the strength of these interactions, have been observed by Dujardin et al.,[5] who found that liquids with surface tension below a threshold value of 130−170 mN/m wet bundles of single-wall carbon nanotubes. A direct experimental observation of the wetting of multiwall CNT by aqueous inclusions composed of 85.2% water, 7.4% CO_2, and 7.4% CH_4 is reported by Gogotsi et al.[6] However, these nanotubes are likely to have numerous defects and attached hydroxyl or carboxyl groups. The conclusion that pure water with a surface tension of 72 mN/m at room temperature should wet CNT is contrasted by the low solubility of CNT in water.[7] For the closely related system of water on graphite surfaces, there is more experimental data available. In 1940, Fowkes[8] measured the contact angle of water on graphite using the tilting plate method and found a value of 86°. A similar result (84°) is reported by Morcos[9] who employed the rising meniscus method for water on pyrolitic graphite. Tadros et al.[10] have used the captive bubble method to find an advancing contact angle of water on graphite of 60−80°. A considerably lower value, namely $42 \pm 7°$, was estimated by Schrader.[11] In a recent scanning force microscopy study, a maximum contact angle of 30° was found for water droplets on graphite exposed to high relative humidity.[12] However, the

authors state that possible contaminations of the surface could influence their results. In the present paper, we compare contact angles obtained from molecular dynamics simulations with the experimental values of both Fowkes[8] (86°) and Schrader[11] (42 $\pm$ 7°).

Molecular dynamics (MD) simulations can be used to complement the experimental data on the CNT−water interaction. The atomically detailed level of description in MD has allowed studies of the properties of water confined inside CNT such as the hydrogen bond network,[13] contact angles,[14] formation of ordered ice nanotubes,[15] spontaneous water conduction[16] and formation of helical ice sheets.[17] The structural characteristics and energetics of water surrounding CNT have also been explored by MD simulations.[18] However, a prerequisite for using MD simulations as a predictive tool in biosensor design is the availability of reliable and validated interaction potentials. In the canonical system of a pristine CNT in water, these potentials include three components, namely a water model, a description of the CNT, and the water−CNT interaction. There exists a variety of water potentials that perform well at standard conditions such as the TIP3P/TIP4P,[19] TIP5P,[20] and SPC/E[21] model and variants thereof.[22] Also for the CNT, elaborate interaction potentials are available.[18,23,24] The key part that requires proper modeling is thus the carbon−water interaction, which determines, in a delicate balance with the water−water interaction, the overall wetting properties of the system.

The aim of the present study is to compare the above listed potentials[13−17] with regard to their ability to predict the static wetting behavior of water on graphite. As a measure thereof, the equilibrium contact angle of water droplets on graphite is used, for which experimental values are available in contrast to the water−CNT system, where no quantitative study of the water−carbon interface has been made. The present MD study reveals that the various interaction potentials lead to qualitatively different wetting behavior.

The outline of this paper is as follows. In section 2, a list is compiled with potentials previously used in MD simulations

---

of water−CNT and water−graphite systems. These potentials are compared by extracting the equilibrium contact angle from MD simulations as explained in section 3. In section 4, the dependence of the contact angle on the drop size and on the interaction potential is discussed. Furthermore, a linear relationship between the contact angle and the parameters of the interaction potential is established that allows us to calibrate the parameters against experimental values. As an illustration, density profiles and hydrogen bond density distribution are presented for a droplet with a contact angle of 86°. The main conclusions are summarized in section 5.

2. Review of Carbon−Water Interaction Potentials in MD Simulations

Molecular dynamics is a well-established tool and the algorithmic details can be found in many textbooks.[25] However, the functional form and parameter values of the underlying force fields are still evolving. A number of force fields have been proposed (e.g., GROMOS,[26] AMBER96,[27] CHARMM,[28] and Brenner[24]), which have been shown to provide accurate predictions for many molecular systems. In this paper, we list interaction potentials that are used in the literature to model CNT−water or graphite−water systems and discuss their ability to describe the macroscopic wetting behavior of water on graphite.

The models are all based on a pairwise additive Lennard-Jones potential between the oxygen atoms of the water and the carbon atoms. The form of this potential is $V(r) = 4\epsilon_{CO}((\sigma_{CO}/r)^{12} - (\sigma_{CO}/r)^6)$, where r is the distance between a pair of carbon and oxygen atoms, ϵ_{CO} is the well depth of the potential, and the parameter σ_{CO} is related to the equilibrium carbon−oxygen distance. Some models also include a carbon−hydrogen LJ interaction[13,17,29] and an electrostatic interaction between the partial charge sites on the water molecules and point quadrupole moments on the carbons.[29]

Bojan and Steele[30] used experimental low-coverage isotherm data of oxygen adsorption on graphite to obtain the carbon−oxygen Lennard-Jones parameters. The values of $\epsilon_{CO} = 0.3135$ kJ mol^{-1} and $\sigma_{CO} = 3.19$ Å resulted from fitting the virial expression using the LJ potential to the experimental data. Marković et al.[29] used these parameters as the base of the water−graphite interaction potential in a combined MD and experimental study of the scattering of water monomers[29] and water clusters[31] on graphite. They increased ϵ_{CO} by 25% to account for the mean contribution of charge induced dipole moments. Furthermore, they added a LJ term between the carbon and the hydrogen atoms with $\epsilon_{CH} = 0.253$ kJ mol^{-1} and $\sigma_{CH} = 2.82$ Å obtained from ref 32 and electrostatic interactions between point quadrupole moments on the carbon and the charges on the oxygen and hydrogen sites as obtained from ref 33. In earlier studies, the authors of the present paper used the LJ parameters given by Bojan and Steele[30] in conjunction with a flexible SPC water model[22] for MD studies of water internal[14] and external[18] to CNTs. However, for consistency with the flexible SPC water model, no carbon−hydrogen LJ term was introduced, and the quadrupole term was neglected because its contribution was found to be insignificant.[18]

Another group of carbon−water potentials is based on parameter values for carbon, oxygen, and hydrogen obtained through the Lorentz−Berthelot mixing rules:

$$\epsilon_{CI} = \sqrt{\epsilon_{CC}\epsilon_{II}} \qquad \sigma_{CI} = \frac{1}{2}(\sigma_{CC} + \sigma_{II}) \qquad I = O, H \quad (1)$$

Gordillo et al.[13] studied the hydrogen bond structure of liquid water confined in carbon nanotubes and also a monolayer of

TABLE 1: References to Recent MD Studies Involving Carbon−Water Interactions[a]

ref	water	E_{pot}	σ_{CO}	ϵ_{CO}	σ_{CH}	ϵ_{CH}	ΔE	h
ref 13	SPC-F2	−41.5[43]	3.280	0.3890	2.81	0.129	−9.70	3.23
ref 16	TIP4P	−41.4[45]	3.275	0.4785			−8.12	3.21
ref 17	TIP3P$_m$	−39.8[44]	3.296	0.5781	2.58	0.323	−16.54	3.23
ref 18	SPC-F1	−45.3[18]	3.190	0.3135			−5.07	3.12
ref 29	SPC	−40.5[44]	3.190	0.3910	2.82	0.253	−12.18	3.11
ref 15	TIP4P	−41.4[45]	3.262	0.3876			−6.53	3.20
present[b]	SPC/E	−47.2[45]	3.190	0.4389			−7.09	3.12

[a] E_{pot} (kJ mol^{-1}) is the bulk energy for the different water models. The Lennard-Jones parameters ϵ_{CO} (kJ mol^{-1}), σ_{CO} (Å), ϵ_{CH} (kJ mol^{-1}), and σ_{CH} (Å) describe the carbon−water interactions. For these potentials, h (Å) is the optimized height and ΔE (kJ mol^{-1}) the binding energy for an SPC/E water monomer above a double layer of graphite. [b] Cf. section 4.

water on a graphite surface by MD simulation.[34] They used a flexible SPC water model[35] with the functional form proposed by Toukan et al.[36] but reparametrized to better reproduce the experimental water infrared spectrum.[37] Their carbon−water interaction parameters $\epsilon_{CO} = 0.389$ kJ mol^{-1}, $\sigma_{CO} = 3.28$ Å, $\epsilon_{CH} = 0.129$ kJ mol^{-1}, and $\sigma_{CH} = 2.81$ Å are based on the mixing rules eq 1 with ϵ_{CC}, σ_{CC}, ϵ_{HH}, and σ_{HH} from ref 38, and ϵ_{OO} and σ_{OO} from ref 39. Koga et al.[15] analyzed a first-order freezing transition of pressurized TIP4P water[19] in a CNT with the carbon−water interactions obtained through the mixing rules (ϵ_{CC} and σ_{CC} from ref 38, ϵ_{OO} and σ_{OO} from ref 19) resulting in parameters of $\epsilon_{CO} = 0.3876$ kJ mol^{-1} and $\sigma_{CO} = 3.262$ Å. In a recent study of water conduction through carbon nanotubes, Hummer et al.[16] used the TIP3P water model[19] and a carbon−oxygen LJ potential with $\epsilon_{CO} = 0.478\,47$ kJ mol^{-1} and $\sigma_{CO} = 3.2751$ Å. The latter parameters correspond to the interaction of sp^2 carbons with oxygen in the AMBER96[27] force field. Hummer et al.[16] also considered a weakened interaction with $\epsilon_{CO} = 0.2703$ kJ mol^{-1} (corresponding to 56.5% of the initial value) and $\sigma_{CO} = 3.4138$ Å. Noon et al.[17] report the formation of helical ice sheets for the modified TIP3P water model TIP3P$_m$[40] in carbon nanotubes under physiological conditions. They use the values of the CHARMM[28] force field: $\epsilon_{CO} = 0.5781$ kJ mol^{-1}, $\sigma_{CO} = 3.296$ Å, $\epsilon_{CH} = 0.3234$ kJ mol^{-1}, and $\sigma_{CH} = 2.584$ Å. Finally, ab initio calculations by Feller and Jordan[41] using second-order Møller−Plesset perturbation theory lead to an estimate of the interaction energy between a water molecule with a single-layer of graphite of 24.27 ± 1.67 kJ mol^{-1}. To recover this energy in MD simulations, a particularly strong Lennard-Jones interaction with parameters of $\sigma_{CO} = 3.2473$ Å and $\epsilon_{CO} = 1.2970$ kJ mol^{-1} [42] is required. An overview of the potentials is listed in Table 1.

To allow a comparison between the different potential models, the binding energy of a water monomer on a double layer of graphite is considered as a representative measure of the strength of the carbon−water interaction. For a fixed bulk water energy, a stronger carbon−water interaction, i.e., a lower binding energy, favors spreading of the water on the graphite and results in a smaller contact angle. On the other hand, a weakening of the carbon−water interaction eventually leads to a hydrophobic system. The binding energies of the different potentials are found to vary considerably with values ranging from −16.72 to −5.19 kJ mol^{-1}; cf. Table 1. To determine the overall wetting properties of the system, one also has to consider the differences in the bulk water energies obtained for different water models. The reported water energies are −41.5, −39.8, −45.3, −40.5, −41.4, and −47.2 kJ mol^{-1} for SPC-F2,[43] TIP3P$_m$,[44] SPC-F1,[18] SPC,[44] TIP4P,[45] and SPC/E[45] water, respectively. In the present study, we employ the rigid SPC/E water model in all simula-

Water−Carbon Interaction Potential

J. Phys. Chem. B, Vol. 107, No. 6, 2003 **1347**

TABLE 2: Overview of the MD Simulations of Water Droplets on Graphite[a]

case	σ_{CO}	ϵ_{CO}	σ_{CH}	ϵ_{CH}	N_{H_2O}	ΔE	r_B	θ (deg)
1	3.190	0.3135			2000	−5.07	25.3	111.3
2[b]	3.190	0.3135			2000	−5.07	25.7	110.0
3[c]	3.190	0.3135			2000		25.3	111.2
4[d]	3.190	0.3135			2000	−5.07	24.3	114.5
5	3.190	0.3135			1000	−5.07	17.7	115.5
6	3.190	0.3135			4000	−5.07	32.5	109.2
7	3.190	0.3135			8379	−5.07	41.8	108.8
8	3.190	0.3135			17576	−5.07	54.0	107.7
9	3.190	0.4389			1000	−7.09	24.2	85.9
10	3.190	0.4389			2000	−7.09	32.8	85.5
11	3.190	0.4389			4000	−7.09	42.2	82.6
12	3.190	0.4389			8379	−7.09	54.4	81.1
13	3.190	0.1881			1000	−3.04	10.9	143.3
14	3.190	0.1881			2000	−3.04	16.4	138.8
15	3.190	0.1881			4000	−3.04	19.5	141.3
16	3.190	0.1881			8379	−3.04	26.9	138.1
17	3.190	0.2508			2000	−4.05	20.1	127.8
18	3.190	0.3762			2000	−6.08	28.2	101.2
19	3.190	0.5016			2000	−8.11	37.4	69.9
20	3.190	0.5643			2000	−9.12	44.6	50.7
21	3.190	0.6270			2000	−10.13	58.0	29.4
22	3.190	0.3910	2.82	0.253	2000	−12.18		0.0
23	3.280	0.3890	2.81	0.129	2000	−9.70	42.4	55.9
24	3.275	0.4785			2000	−8.12	39.4	65.4
25	3.296	0.5781	2.58	0.323	2000	−16.54		0.0
26[e]	3.275	0.4785			2000	−8.12	46.7	48.0
27	3.296	0.4389			2000	−7.53	35.6	76.8
28	3.190	0.3920			2000	−6.33	30.1	95.3

[a] The water−carbon interaction is modeled through Lennard-Jones potentials with parameters ϵ_{CO} (kJ mol^{-1}), σ_{CO} (Å), ϵ_{CH} (kJ mol^{-1}), and σ_{CH} (Å). The resulting binding energy of a water molecule on a double layer of graphite is denoted by ΔE (kJ mol^{-1}). N_{H_2O} is the number of water molecules in the droplets, and r_B and θ are the droplet base radius and the contact angle as obtained from the simulation. [b] Case 1 with a cutoff radius of 25 Å for the electrostatics. [c] Case 1 with flexible graphite. [d] Case 1 with different initial conditions. [e] Case 24 with the TIP3P water model.

tions. Note that the simulations carried out with a different water model would yield contact angles different from the ones reported here. However, the contact angles obtained with the SPC/E model present an upper bound because the SPC/E water model has the lowest bulk energy.

3. Methodology

To study the sensitivity of the contact angle to the carbon−water interaction potential and the droplet size, a series of MD simulations of water droplets on graphite is performed, as specified in Table 2. In the following, the MD simulation technique is described along with the details on how the contact angles, density profiles, hydrogen bond distributions, and line tension are extracted from the simulations.

3.1. Molecular Dynamics Simulations. The reference water model in this study is the rigid extended Simple Point Charge potential SPC/E.[21] It consists of a smoothly truncated Coulomb potential[46] acting between partial point charges on the oxygen (−0.8476e) and hydrogen (+0.4238e) atoms and an O−O Lennard-Jones interaction with $\epsilon_{OO} = 0.6502$ kJ mol^{-1} and $\sigma_{OO} = 3.166$ Å. The SHAKE algorithm[47] is used to keep the O−H distance fixed at 1 Å and the H−O−H angle at 109.47°.

In all but one of the simulations, the graphite atoms are fixed at their respective initial positions and represent an inert wall; cf. ref 48. The exception is the validation case 4 where the carbon atoms interact via a Morse bond potential, a harmonic angle potential, a torsion potential, and a carbon−carbon LJ interaction, as described in ref 18. It will be shown that fixing
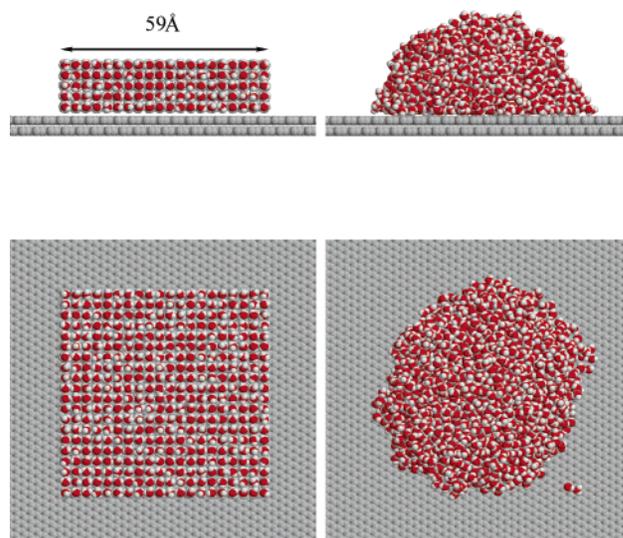

Figure 1. Side (top row) and top view (bottom row) of the initial ($t = 0$) and equilibrated ($t = 0.2$ ns) water droplets in case 28. The views are close-ups; the lateral graphite dimensions in this simulation are 119×118 Å.

the carbon atoms does not affect the contact angle of the droplets, but it does reduce the computational expense significantly. The horizontal extent of the graphite is 119×118 Å or 200×200 Å, depending on the droplet size to effectively remove the periodic images of the droplets. The graphite consists of two staggered sheets with an interlayer distance of 3.4 Å. Additional sheets of graphite were omitted because they are not expected to have a significant influence on the water due to the employed cutoff radius of 10 Å.

For most of the simulations considered, the water−carbon interaction is solely based on an oxygen−carbon Lennard-Jones potential in which σ_{CO} is kept fixed at 3.19 Å while ϵ_{CO} is systematically varied in the range 0.1881 to 0.6270 kJ mol^{-1}. Additionally, several potentials recently used in the literature (cf. Table 1) as well as a test case with a different σ_{CO} value and one with a different water model are considered. A more detailed description of the individual cases is given in section 4 and a summary of all simulated cases is compiled in Table 2.

The simulations in the present work are performed using the parallel molecular dynamics code FASTTUBE.[14,18] All simulations are carried out for 1 ns with an integration time step of 2 fs and a cutoff radius of 10 Å for all potentials except for case 2 where a cutoff of 25 Å is applied. In the first half of the 200 ps equilibration time, the system is coupled to a Berendsen thermostat at a temperature of 300 K, whereas in the second half of the equilibration and for the sampling a constant energy simulation is performed. The water temperature remains stable during the production runs, e.g., for case 10, it has an average of 299.9 K and a standard deviation of 5.0 K. The water molecules are initially placed on a regular lattice; cf. the illustration of an initial and an equilibrated configuration in Figure 1. Samples of the trajectory are stored every 0.2 ps.

3.2. Diagnostics. From the MD simulation trajectories, water isochore profiles are obtained by introducing a cylindrical binning, which uses the topmost graphite layer as zero reference level and the surface normal through the center of mass of the droplet as reference axis. The bins have a height of 0.5 Å and are of equal volume, i.e., the radial bin boundaries are located at $r_i = \sqrt{i\delta A/\pi}$ for $i = 1, ..., N_{bin}$ with a base area per bin of $\delta A = 95$ Å^2. To extract the water contact angle from such a profile, a two-step procedure is adopted, as described by de Ruijter et
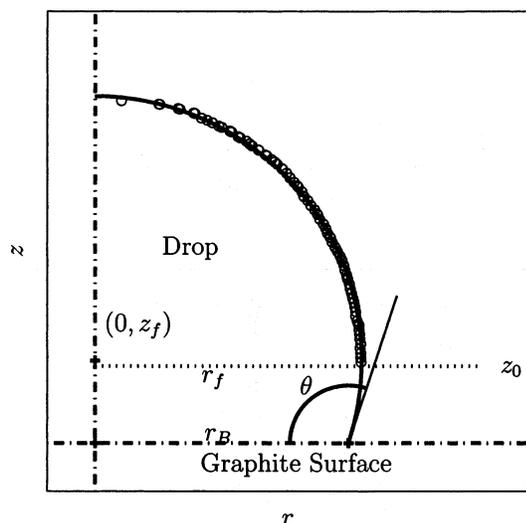
Figure 2. Contact angle measured by fitting a circle with center (0, z_f) and radius r_f to the points of the equimolar dividing plane (circles) with $z > z_0 = 8$ Å to exclude the near wall region. The droplet has a base radius r_B.

al.[49] First, the location of the equimolar dividing surface is determined within every single horizontal layer of the binned drop. Second, a circular best fit through these points is extrapolated to the graphite surface where the contact angle θ is measured; cf. Figure 2. Note that the points of the equimolar surface below a height of 8 Å from the graphite surface are not taken into account for the fit, to avoid the influence from density fluctuations at the liquid−solid interface. The contact angle depends only weakly on this choice, e.g., for case 10, it is reduced by 1.0° if all points off the equimolar surface are included ($z_0 = 0$ in Figure 2). Furthermore, only those points are used for which the density measured in the central bin lies within a range of 0.5−1.1 g cm^{-3}. This effectively excludes the points in the cap region where statistics are poor; cf. also Figure 9.

The same binning procedure as for the water density is applied to compute the hydrogen bond density distribution within the droplet. To count the hydrogen bonds (HB), the geometrical criterion proposed by Martí[50] is used. Thus, two water molecules are hydrogen bonded if their oxygen atoms are within 3.6 Å of each other and if the distance between the oxygen and the hydrogen that form the HB is less than 2.4 Å. Additionally, it is required that the angle formed by the oxygen−oxygen direction and the molecular oxygen−hydrogen bond, where the latter hydrogen is in the HB, is less than 30°.

The macroscopic contact angle θ_∞ is related to the microscopic contact angle θ through the modified Young's equation; see, e.g., ref 51. It relates the surface tensions γ of the relevant phases (subscripts S, L, and V for solid, liquid, and vapor phase, respectively) and the line tension τ with the contact angle θ and the droplet base radius r_B (see Figure 2) as

$$\gamma_{SV} = \gamma_{SL} + \gamma_{LV} \cos \theta + \frac{\tau}{r_B} \qquad (2)$$

Young's equation is recovered for macroscopic droplets, i.e., for $1/r_B \rightarrow 0$. In that case, the macroscopic contact angle θ_∞ is defined as $\cos \theta_\infty = (\gamma_{SV} - \gamma_{SL})/\gamma_{LV}$, and (2) can be rewritten as

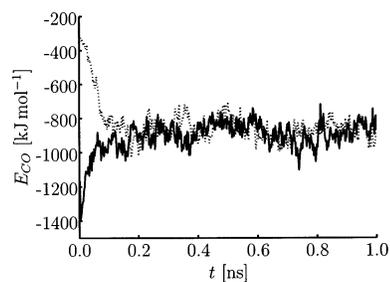$$\cos \theta = \cos \theta_\infty - \frac{\tau}{\gamma_{LV}} \frac{1}{r_B} \qquad (3)$$

Figure 3. Total carbon−oxygen Lennard-Jones interaction energy for the cases 1 (—) and 4 (···), which only differ in the initial arrangement of the water molecules. The mean values of the energies, measured for $t > 0.2$ ns, are −884.1 and −861.0 kJ mol^{-1} for the cases 1 and 4, respectively.

where the cosine of the microscopic contact angle is linearly related to the droplet base curvature $1/r_B$.

4. Results and Discussion

Three validation studies (cases 2−4, cf. Table 2) were conducted to assess the influence of the initial and boundary conditions, and of the adjustable parameters of the computational model, on the observed contact angle. For this, the first simulation (case 1) served as a reference case with a 2000 water molecule droplet and with Lennard-Jones interaction parameters of $\epsilon_{CO} = 0.3135$ kJ mol^{-1} and $\sigma_{CO} = 3.19$ Å. The value of the contact angle was found to be 111.3° for the reference case 1. The sensitivity of the contact angle was investigated with regard to the following modifications. First, the cutoff radius for the electrostatic interaction was increased from 10 to 25 Å in case 2, which led to a slightly decreased contact angle of 110.0°. Next, the flexible graphite interaction potential was employed (case 3) instead of modeling graphite as an inert wall. The resulting change in the contact angle was only 0.1° and therefore negligible. Finally, a different initial geometry was used with the water molecules arranged on a $10 \times 10 \times 20$ (case 4) instead of a $20 \times 20 \times 5$ lattice, leading to a contact angle of 114.5°. The equilibration of the carbon−oxygen Lennard-Jones energy of the latter two cases is shown in Figure 3. The mean values of the energies, measured for $t > 200$ ps, are −884.1 and −861.0 kJ mol^{-1} for the cases 1 and 4, respectively, which is consistent with the difference in the observed contact angle. The low-frequency oscillations present in the time history of the carbon−oxygen energy (cf. Figure 3) are ascribed to capillary waves at the surface of the drop.[52] The contact angles of the three validation runs lie within ±3° of the reference run 1, which is acceptable in the present work and justifies the choice of a 10 Å cutoff and the inert graphite. We shall see that the variation in the LJ interaction parameters considered here, results in qualitatively different contact angle values.

4.1. Dependence of the Contact Angles on the Drop Size. According to the modified Young's eq 3, the microscopic contact angle θ deviates from the macroscopic angle θ_∞ due to the line tension τ. The effect of a positive line tension is to contract the droplet base and to increase the contact angle whereas a negative τ enhances wetting. However, as τ is believed to be on the order of 10^{-10} J/m,[53] the line tension is only expected to be significant for droplets with diameters below 10 nm — a length scale where quantitative measurements are difficult to carry out. The requirements for a precise experimental determination of τ include an accurate contact angle measuring technique and the use of a highly purified liquid on an atomically smooth surface. These requirements are perfectly matched in MD simulations, as is the necessary length scale.
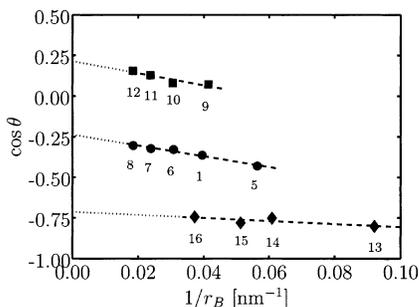
Water−Carbon Interaction Potential

J. Phys. Chem. B, Vol. 107, No. 6, 2003 **1349**

Figure 4. Cosine of the contact angle θ as a function of the droplet base curvature $1/r_B$. The three series are computed using Lennard-Jones parameters of $\epsilon_{CO} = 0.3135$ kJ mol^{-1} (circles), $\epsilon_{CO} = 0.4389$ kJ mol^{-1} (squares), and $\epsilon_{CO} = 0.1881$ kJ mol^{-1} (diamonds) for droplets with an increasing number of water molecules: 1000 (cases 5, 13, and 9), 2000 (cases 1, 14, and 10), 4000 (cases 6, 15, and 11), 8379 (case 7, 16, and 12), and 17576 (case 8).

A straightforward method to determine the effect of the line tension τ in MD simulations is to measure the contact angle θ and the contact line curvature $1/r_B$ for droplets of different sizes. Here, three series of simulations were considered within each of which the carbon−water interaction parameters are identical, but the drop sizes vary. In the first series, an interaction potential with $\epsilon_{CO} = 0.3135$ kJ mol^{-1} and $\sigma_{CO} = 3.19$ Å was applied to droplets with respective sizes of 1000, 2000, 4000, 8379, and 17 576 water molecules (cases 5, 1, and 6−8). For comparison: Free-standing spherical droplets with the same number of waters have respective radii of 19.3, 24.3, 30.6, 39.1, and 50.1 Å when a uniform density of 0.997 g cm^{-3} is assumed. For the second series, the interaction parameter ϵ_{CO} was increased by 40% ($\epsilon_{CO} = 0.4389$ kJ mol^{-1}) for droplets of 1000, 2000, 4000, and 8379 water molecules (cases 9−12). Finally, in the third series, a weaker interaction with ϵ_{CO} decreased by 40% ($\epsilon_{CO} = 0.1881$ kJ mol^{-1}) was used to simulate similar size droplets (cases 13−16).

In Figure 4, the cosine of the contact angle θ is plotted as function of the curvature of the droplet base radius $1/r_B$ for all the simulations. Included in Figure 4 are linear fits to each series of data points (dashed lines). Extending these linear fits to the limit of infinitely large droplets ($1/r_B \rightarrow 0$) results in macroscopic contact angles (θ_∞) of 135.5°, 103.7°, and 77.6°, for the weak, the standard, and the stronger interaction potential, respectively. We note (cf. Table 2) that these extrapolated contact angles differ from those obtained for the simulated droplets. In fact, the differences between the macroscopic contact angle and the contact angle for the 2000 water molecule droplet were −3.3°, −7.6°, and −7.9° (cases 14, 1, and 10), indicating a slight contraction of the droplet base, and thus a positive line tension. The magnitude of the line tension can be estimated from the slopes of the fits in Figure 4, cf. eq 3, which are −0.94 nm (case 14), −3.33 nm (case 1), and −3.72 nm (case 10), respectively. For a surface tension of water of $\gamma_{LV} = 72$ mN/m, the line tension τ is found to be 0.7×10^{-10} J/m (case 14), 2.4×10^{-10} J/m (case 1), and 2.7×10^{-10} J/m (case 10). These values are in agreement with a recent atomic microscopy study by Mugele[53] where liquid droplets of different sizes (0.38−8μm) were imaged to determine the contact line tension. All the following simulations are carried out for the 2000 water molecule droplet. However, in the subsequent calibration of the interaction potential parameters, the line tension is taken into account by adjusting the target value from 86°,[8] i.e., from the macroscopically observed one, to its microscopic, rounded, counterpart of 94°. Similarly, the target value of 42°[11] is shifted

to 50°, assuming that the effect of the line tension is the same for this case.

4.2. Dependence of the Contact Angles on the Interaction Potentials. The considered graphite−water interactions include a carbon−oxygen Lennard-Jones potential for which the parameter ϵ_{CO} is systematically increased from a value of 0.1881 to 0.6270 kJ mol^{-1} in increments of 0.0627 kJ mol^{-1}. As expected, the linear increase of ϵ_{CO} leads to a monotonic decrease in the observed microscopic contact angle, cf. Figure 6. In order of increasing ϵ_{CO}, the simulations resulted in contact angles of 138.8°, 127.8°, 111.3°, 101.2°, 85.5°, 69.9°, 50.7°, and 29.4°, respectively (cases 14, 17, 1, 18, 10, 19, 20, and 21). The transition from the nonwetting ($\theta > 90°$) to the wetting behavior ($\theta < 90°$) occurs for an ϵ_{CO} in the range between 0.3762 and 0.4389 kJ mol^{-1}.

Complementary simulations were performed using the water−carbon interaction potentials from the literature listed in Table 1. Note that the rigid SPC/E water model was used in all our simulations, independently of the choice of water model in the original studies. The first potential in Table 1 includes a carbon−oxygen interaction with $\epsilon_{CO} = 0.389$ kJ mol^{-1} and a carbon−hydrogen LJ potential with $\epsilon_{CH} = 0.129$ kJ mol^{-1} (case 23). For this case, the contact angle is found to be 55.9°. The second potential (case 24) has a stronger carbon oxygen interaction with $\epsilon_{CO} = 0.4785$ kJ mol^{-1}, but the absence of a carbon−hydrogen interaction results in a larger contact angle of 65.4°. The strongest interaction considered is the potential used in ref 17 (case 25), where the droplet interacts with the graphite through LJ potentials with $\epsilon_{CO} = 0.5781$ and $\epsilon_{CH} = 0.323$ kJ mol^{-1}. This simulation results in a monolayer of water and thus a contact angle of 0°. Finally, for the fourth potential with $\epsilon_{CO} = 0.3910$ and $\epsilon_{CH} = 0.253$ kJ mol^{-1} (case 22), the initial configuration relaxed to two adsorbed layers of water, which essentially corresponds to a vanishing contact angle. Note that for simplicity, but in contrast to the original work in ref 29, no electrostatic interactions were included between the water and the carbon for case 22. In view that the contact angle vanished without this contribution, this approximation is justifiable.

In the following comparisons, each water−graphite potential is solely characterized through the binding energy ΔE of a water monomer on graphite, which is independent of the functional form of the potential and reflects the attraction of a water molecule to the basal plane of graphite. This single molecule binding energy is a sufficient measure of the attraction of a water droplet to a graphitic substrate because it is revealed to be proportional to the total carbon−water energy. In fact, the carbon−oxygen Lennard-Jones energy per unit area of the droplet footprint E_{CO} is found to scale linearly with the parameter ϵ_{CO}, as evidenced by Figure 5, where ϵ_{CO} is plotted against E_{CO} for the cases 14, 17, 1, 18, 10, 19, 20, and 21. A significant discrepancy from the linear relation is observed only for case 21. We believe the large footprint of the droplet (due to its contact angle of 29.4°) and the small number of water molecules (2000) does not allow the interior of the droplet to reach bulk properties.

To compute the binding energy ΔE of a water monomer for the different potentials, a covariance adaptation matrix minimization technique[54] is used. The resulting energies and the respective heights of the oxygen atoms above the graphite surface are included in Table 2. The initial position is chosen at random and during the minimization, no constraints are applied on the position or orientation of the water molecule. For the cases without a C−H potential, this conformation corresponds to having the oxygen atom centered above a
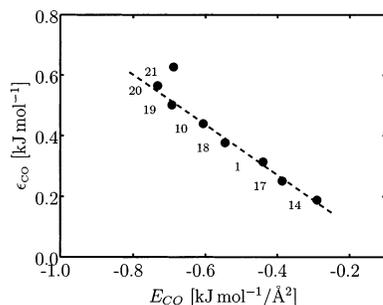
Figure 5. Relation between the Lennard-Jones parameter ϵ_{CO} and the total water−carbon interaction energy per unit area of the droplet footprint. The interaction potentials for the different case numbers are detailed in Table 2. The dashed line is a linear fit to the data points excluding the case 21.
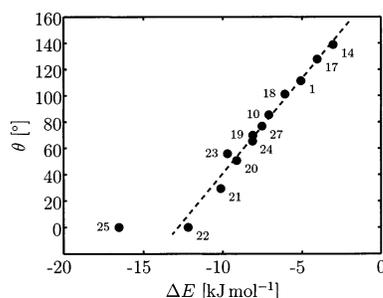

Figure 6. Contact angle θ of water droplets on graphite as a function of the binding energy ΔE of a single water molecule. The interaction potentials for the different case numbers are detailed in Table 2. The dashed line is a linear fit excluding the cases 22, 25, and 27.

hexagon at the heights given in Table 1. The cases including a C−H term have the oxygen slightly off the hexagon center (<0.2 Å), and the hydrogens pointing down. The relation between the water contact angle θ and the water monomer binding energy ΔE on graphite is depicted in Figure 6. The dashed line in Figure 6 is a linear fit to all data points with nonzero contact angle, i.e., excluding the cases 22 and 25. The fit has the form

$$\theta = 185.8° + \Delta E \cdot 14.5°(\text{kJ mol}^{-1})^{-1} \qquad (4)$$

and intersects the $\theta = 0°$ line at a binding energy of $\Delta E_c = -12.82$ kJ mol^{-1}. According to the linear relation suggested in Figure 6, any binding energy below a critical value ΔE_c will result in a complete wetting of the graphite surface. In fact, case 22 with a binding energy $\Delta E = -12.18$ kJ mol^{-1} (not included in the fit) stabilized in a 2−3 molecule thick water layer, i.e., just before complete wetting, which is in excellent agreement with the prediction of $\Delta E_c = -12.82$ kJ mol^{-1}. An extrapolation of the fit to a vanishing interaction energy ($\Delta E = 0$) between the water and the graphite leads to a contact angle of 185.8°, which is reasonably close to the limiting value of 180.0°. The only case that includes a carbon−hydrogen Lennard-Jones term and has a nonvanishing contact angle (case 23) is slightly off the linear fit in Figure 6. This can be explained by observing that the average orientation of the water molecules close to the water−graphite interface is not the optimal one that is used to calculate the monomer binding energy. Above the threshold of $\Delta E_c = -12.82$ kJ mol^{-1}, one can, for a given carbon−water interaction potential, predict the equilibrium contact angle if the binding energy of a water monomer on graphite is known. Inversely, one can choose to match a prescribed contact angle by adjusting the water monomer binding energy (ΔE) according to eq 4. For the first target
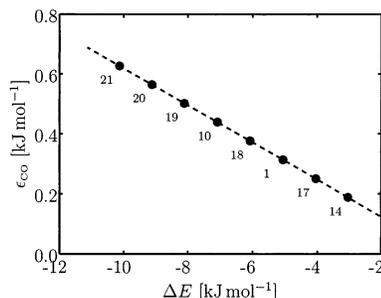

Figure 7. Relation between the Lennard-Jones parameter ϵ_{CO} and the water monomer binding energy ΔE on graphite. The interaction potentials for the different case numbers are detailed in Table 2. The dashed line is a linear fit to all data points.

contact angle value of 94° (cf. section 4.1) this binding energy amounts to −6.33 kJ mol^{-1} and for the second target value of 50°, it amounts to −9.37 kJ mol^{-1}.

The final step is to adopt a functional form for the graphite−water potential and to determine the parameters that yield the desired monomer binding energy. For the present study, a simple carbon−oxygen Lennard-Jones potential is chosen with the characteristic length σ_{CO} fixed at 3.19 Å. In Figure 7, the parameter ϵ_{CO} is plotted as a function of ΔE for the potential parameters used in the simulations 1, 10, 14, and 17−21, respectively. The dashed line in Figure 7 is a fit to the data points and has the form

$$\epsilon_{CO} = -0.0619\Delta E \qquad (5)$$

Thus, to obtain a binding energy of −6.33 kJ mol^{-1} requires an ϵ_{CO} of 0.392 kJ mol^{-1}, i.e., a 25% larger value than in the potential used in earlier simulations by the authors.[14,18] This increase may be interpreted as an average contribution from the induced electrostatic interactions between that water and the graphite or the C−H interactions that are not treated explicitly in the present approach. But it is also conceivable that the increase reflects a flaw in the transferability of molecular oxygen adsorption measurements to water. A detailed analysis of a simulation where this new potential is applied to a 2000 water molecule droplet on graphite (case 28) is discussed below. For the second target value of 50°, the relation (5) suggests using an ϵ_{CO} of 0.5797 kJ mol^{-1}, which is in good agreement with case 20, where the choice $\epsilon_{CO} = 0.5643$ kJ mol^{-1} leads a contact angle of 50.7°.

In the following, we discuss the implications on the relations (4) and (5) of having used the SPC/E water model and having fixed $\sigma_{CO} = 3.19$ Å for all the cases. Different water models do not produce the same bulk water energy, which is, for a constant water−carbon interaction, equivalent to shifting the energy balance between the water−carbon and water−water interactions. The bulk water energies reported in the literature are listed in Table 1. However, because the SPC/E water model possesses the lowest energy of these models, the contact angle values reported here constitute upper bounds to those that one would obtain for water models with weaker water−water interactions. As an example, the contact angle for the case 24 is lowered from 65.4° to 48.0° if the SPC/E is replaced with the TIP3P water model (case 26). To investigate the influence of σ_{CO} on the contact angle, case 27 was introduced, which is identical to case 10 except for an increased σ_{CO} value of 3.29 Å, corresponding to the largest value found in the literature, cf. Table 1. For case 27 (case 10), we find a contact angle of 76.8° (85.3°) and a monomer water binding energy on graphite of −7.53 kJ mol^{-1} (−7.09 kJ mol^{-1}). The ratio of the contact angle
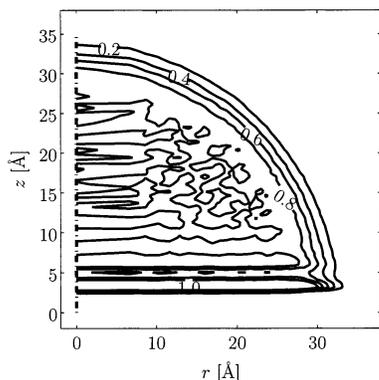
J. Phys. Chem. B, Vol. 107, No. 6, 2003 **1351**

Figure 8. Time averaged water isochore profile for case 28; cf. Table 2. The isochore levels are 0.2, 0.4, 0.6, 0.8, and 1.0 g cm^{-3}. The density profile along the centerline of the droplet is shown in Figure 9.

and the monomer binding energy is in remarkable agreement with the rest of the calculations, as evidenced by Figure 6.

In summary, the interaction potentials recently used for studies of water−graphite and water−carbon nanotube systems have shown a large variation in the strength of the water−carbon interaction. Employing these potentials to the model problem of a water droplet on graphite results in qualitatively different behavior ranging from a strongly hydrophilic to hydrophobic interface. The observed differences are expected to impact the results of earlier studies such as the scattering of water droplets on graphite,[55] and water internal[14] and external to carbon nanotubes.[18] In particular, the formation of ice like structures in carbon nanotubes observed in ref 17 could be caused by the applied strong interaction potential.

4.3. Water Density and Hydrogen Bond Distribution Profiles. In this section, we present water density profiles and hydrogen bond distributions for the water−carbon interaction parameters $\epsilon_{CO} = 0.392$ kJ mol^{-1} and $\sigma_{CO} = 3.19$ Å (case 28). It was predicted (cf. section 4.2) that these parameters lead to a microscopic contact angle of 94° for a 2000 water molecule droplet (rigid SPC/E water) on a double layer of graphite. The simulation results in a contact angle of 95.3°, which is in good agreement with the expected value. The average water density profile is shown in Figure 8 in the form of a contour plot with isochores at levels of 0.2, 0.4, 0.6, 0.8, and 1.0 g cm^{-3}, respectively. Note that the layered structure of the liquid close to the wall ($0 < z < 8$ Å) is neglected in the contact angle measurement. A density profile along the centerline of the droplet in Figure 8 is depicted in Figure 9. To resolve this profile, the bin size in the z direction was refined to 0.125 Å. Close to the graphite, two pronounced density peaks can be identified at distances of 3.2 and 6.2 Å with peak heights of 2.74 and 1.30 g cm^{-3}, respectively. The density profile from the bulk water region across the liquid−vapor interface ($z > 10$ Å) fits the hyperbolic tangent functional form

$$\rho(z) = \frac{\rho_l}{2}\left(1 - \tanh\left(\frac{2(z - z_e)}{d}\right)\right) \qquad (6)$$

where the vapor density is assumed to be zero, ρ_l is the density of the bulk liquid, z_e the height, and d a measure for the width of the liquid−vapor interface. A fit of eq 6 to the profile obtained for case 28 (cf. Figure 9) yields a bulk liquid density of $\rho_l = 0.999$ g cm^{-3} and $d = 4.3$ Å, resulting in an interface thickness of 4.8 Å (the interface thickness is here defined as the region where the water density drops from $0.9\rho_l$ to $0.1\rho_l$).

A contour plot of the hydrogen bond density of case 28 is shown in Figure 10. The HB density along the z-axis in the
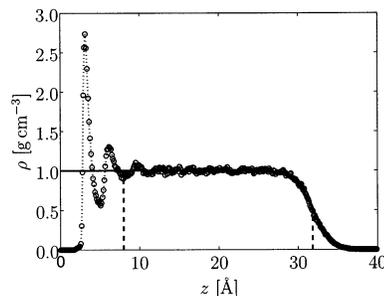

Figure 9. Density profile for case 28 along the centerline of the droplet; cf. Figure 8. The full line is a fit to the density using the functional form of eq 4. For the calculation of the contact angle, only the data points contained within the vertical dashed lines are used ($z > 8$ Å and z : $0.5 < \rho(z) < 1.1$ g cm^{-3}).
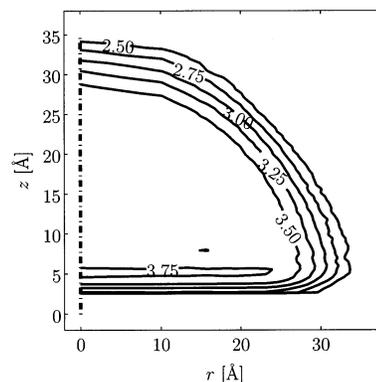

Figure 10. Average number of hydrogen bonds per water molecule for the droplet in case 28; cf. Table 2. The isolines are at levels of 2.50, 2.75, 3.00, 3.25, 3.50, and 3.75 hydrogen bonds. The profile along the centerline of the droplet is shown in Figure 11.
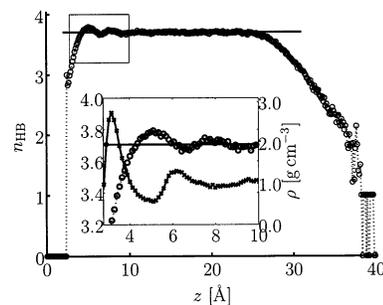

Figure 11. Vertical hydrogen bond distribution profile for case 28; cf. Table 2. Displayed is the average hydrogen bond number in the central bin, i.e., the number of hydrogen bonds along the dashed line in Figure 10. The inset is a magnified view of the hydrogen bond number (circles) and density (crosses) at the water graphite interface.

central part of the droplet is given in Figure 11. In the bulk region (10 Å < z < 25 Å) an averaged number of hydrogen bonds of 3.70 per water molecule is found, which is in reasonable agreement with the experimental value of 3.9[56] and with previous MD studies.[13,18] The HB density profile of case 28 exhibits distinct extrema at locations similar to those observed in the water density profiles. At the first maximum, the average HB number per water molecule is 3.79 (3.0% above the mean value) whereas at the first minimum there are 3.66 and at the second maximum 3.75 HBs per water molecule. The inset in Figure 11 combines the water density and the hydrogen bond density profile close to the wall and shows the correlation between the peaks of the density with those of the HB density. The noisy behavior of the HB density for $z > 35$ Å is attributed to the poor statistics in this low-density region; cf. also Figure 9.

1352 *J. Phys. Chem. B, Vol. 107, No. 6, 2003*

Werder et al.

5. Conclusions

We have presented a systematic study of the potential functions commonly used to model the interaction between water and graphite (or carbon nanotubes) in molecular dynamics simulations. The contact angle of a water droplet on graphite has served as a measure of the energy balance between the water−water and the water−carbon interaction. The results indicate that a binding energy of a water monomer on graphite below a threshold of $\Delta E_c = -12.82$ kJ mol^{-1}, leads to complete spreading of a water droplet. Water monomer binding energies of -6.33 and -9.37 kJ mol^{-1} are required to recover, in the macroscopic limit, contact angles of 86°[8] and 42°,[11] respectively. These binding energies include a correction to account for the line tension which, through MD simulations of droplets of different sizes, is estimated to be positive and on the order of 2×10^{-10} J/m. For a simple Lennard-Jones interaction potential acting between the oxygen atoms of the water and the carbon atom sites, the corresponding interaction parameters to obtain the desired binding energies are $\sigma_{CO} = 3.19$ Å and $\epsilon_{CO} = 0.392$ and 0.5643 kJ mol^{-1}, respectively. A calibration of a water−graphite potential that includes a carbon−hydrogen interaction is part of future work.

References and Notes

(1) Tombler, T. W.; Zhou, C.; Alexseyev, L.; Kong, J.; Dai, H.; Jayanthi, C. S.; Tang, M.; Wu, S.-Y. *Nature* **2000**, *405*, 769−772.

(2) Kong, J.; Franklin, N. R.; Zhou, C.; Chapline, M. G.; Peng, S.; Kyeongjae, C.; Dai, H. *Science* **2000**, *287*, 622−625.

(3) Erlanger, B. F.; Chen, B.-X.; Zhu, M.; Brus, L. *Nano Lett.* **2001**, 465−467.

(4) Huang, W.; Taylor, S.; Fu, K.; Lin, Y.; Zhang, D.; Hanks, T. W.; Rao, A. M.; Sun, Y.-P. *Nano Lett.* **2002**, *2* (4), 311−314.

(5) Dujardin, E.; Ebbesen, T. W.; Krishnan, A.; Treacy, M. M. J. *Adv. Mater.* **1998**, *10* (17), 1472−1475.

(6) Gogotsi, Y.; Libera, J. A.; Güvenç-Yazicioglu, A.; Megaridis, C. M. *Appl. Phys. Lett.* **2001**, *79* (7), 1021−1023.

(7) Bahr, J. L.; Mickelson, E. T.; Bronikowski, M. J.; Smalley, R. E.; Tour, J. M. *Chem. Commun.* **2001**, *2*, 193−194.

(8) Fowkes, F. M.; Harkins, W. D. *J. Am. Chem. Soc.* **1940**, *62*, 2 (12), 3377−3377.

(9) Morcos, I. *J. Chem. Phys.* **1972**, *57* (4), 1801−1802.

(10) Tadros, M. E.; Hu, P.; Adamson, A. W. *J. Colloid Interface Sci.* **1974**, *49* (2), 184−195.

(11) Schrader, M. E. *J. Phys. Chem.* **1980**, *84*, 2774−2779.

(12) Luna, M.; Colchero, J.; Baró, A. M. *J. Phys. Chem. B* **1999**, *103*, 9576−9581.

(13) Gordillo, M. C.; Martí, J. *Chem. Phys. Lett.* **2000**, *329*, 341−345.

(14) Werder, T.; Walther, J. H.; Jaffe, R.; Halicioglu, T.; Noca, F.; Koumoutsakos, P. *Nano Lett.* **2001**, *1* (12), 697−702.

(15) Koga, K.; Gao, G. T.; Tanaka, H.; Zeng, X. C. *Nature* **2001**, *412*, 802−805.

(16) Hummer, G.; Rasaiah, J. C.; Noworyta, J. P. *Nature* **2001**, *414*, 188−190.

(17) Noon, W. H.; Ausman, K. D.; Smalley, R. E.; Ma, J. *Chem. Phys. Lett.* **2002**, *355*, 445−448.

(18) Walther, J. H.; Jaffe, R.; Halicioglu, T.; Koumoutsakos, P. *J. Phys. Chem. B* **2001**, *105*, 9980−9987.

(19) Jorgensen, W. L.; Chandrasekhar, J.; Madura, J. D.; Impey, R. W.; Klein, M. L. *J. Chem. Phys.* **1983**, *79* (2), 926−935.

(20) Mahoney, M. W.; Jorgensen, W. L. *J. Chem. Phys.* **2000**, *112* (20), 8910−8922.

(21) Berendsen, H. J. C.; Grigera, J. R.; Straatsma, T. P. *J. Phys. Chem.* **1987**, *91*, 6269−6271.

(22) Teleman, O.; Jönsson, B.; Engström, S. *Mol. Phys.* **1987**, *60* (1), 193−203.

(23) Che, J.; Cagin, T.; Goddard, W., III. *Nanotechnology* **1999**, *10*, 263−268.

(24) Brenner, D. W. *Phys. Rev. B* **1990**, *42* (15), 9458−9471.

(25) Allen, M. P.; Tildesley, D. J. *Computer Simulation of Liquids*; Clarendon Press Oxford: Oxford, U.K., 1987.

(26) van Gunsteren, W. F.; Billeter, S. R.; Eising, S. R.; Hünenberger, P. H.; Krüger, P.; Mark, A. E.; Scott, W. R. P.; Tironi, I. G. *Biomolecular Simulation: The GROMOS96 Manual and User Guide*; Vdf Hochschulverlag AG: Zürich, Switzerland, 1996.

(27) Cornell, W. D.; Cieplak, P.; Bayly, C. I.; Gould, I. R.; Merz, Jr., K. M.; Ferguson, D. M.; Spellmeyer, D. C.; Fox, T.; Caldwell, J. W.; Kollman, P. A. *J. Am. Chem. Soc.* **1995**, *117*, 5179−5197.

(28) Brooks, B. R.; Bruccoleri, R. E.; Olafson, B. D.; States, D. J.; Swaminathan, S.; Karplus, M. *J. Comput. Chem.* **1983**, *4* (2), 187−217.

(29) Marković, N.; Andersson, P. U.; Någård, M. B.; Petterson, J. B. C. *Chem. Phys.* **1999**, *247*, 413−430.

(30) Bojan, M. J.; Steele, W. A. *Langmuir* **1987**, *3* (6), 1123−1127.

(31) Tomsic, A.; Anderson, P. U.; Markovic, W.; Svanberg, M.; Pettersson, J. B. C. *J. Chem. Phys.* **2001**, *115* (22), 10509−10517.

(32) Cheng, A.; Steele, W. A. *J. Chem. Phys.* **1990**, *92* (6), 3858−3866.

(33) Vernov, A.; Steele, W. A. *Langmuir* **1992**, *8*, 155−159.

(34) Gordillo, M. C.; Martí, J. *J. Chem. Phys.* **2002**, *117* (7), 3425−3430.

(35) Martí, J.; Padró, J. A.; Guàrdia, E. *J. Chem. Phys.* **1996**, *105* (2), 639−649.

(36) Toukan, K.; Rahman, A. *Phys. Rev. B* **1985**, *31* (5), 2643−2648.

(37) Martí, J.; Padró, J. A.; Guàrdia, E. *J. Mol. Liq.* **1994**, *62*, 17−31.

(38) Steele, W. A. *The Interaction of Gases With Solid Surfaces*; Pergamon Press: Oxford, U.K., 1974.

(39) Berendsen, H. J. C.; Postma, J. P. M.; van Gunsteren, W. F.; Hermans, J. In *Intermolecular Forces*; Pullman, B., Ed.; Reidel: Dordrecht, The Netherlands, 1981; pp 331−342.

(40) Neria, E.; Fischer, S.; Karplus, M. *J. Chem. Phys.* **2002**, *105* (5), 1902−1921.

(41) Feller, D.; Jordan, K. D. *J. Phys. Chem. A* **2000**, *104*, 9971−9975.

(42) Jaffe, R. L. Technical report, NASA Ames Reseach Center, 2001.

(43) Gordillo, M. C.; Martí, J. *Chem. Phys. Lett.* **2001**, *341*, 250−254.

(44) Mark, P.; Nilsson, L. *J. Phys. Chem. A* **2001**, *105*, 9954−9960.

(45) van der Spoel, D.; van Maaren, P. J.; Berendsen, H. J. C. *J. Chem. Phys.* **1998**, *108* (24), 10220−10230.

(46) Levitt, M.; Hirshberg, M.; Laidig, K. E.; Daggett, V. *J. Phys. Chem. B* **1997**, *101*, 5051−5061.

(47) Ryckaert, J.-P.; Cicotti, G.; Berendsen, H. J. C. *J. Comput. Phys.* **1977**, *23*, 327−341.

(48) Nijmeijer, M. J. P.; Bruin, C.; Bakker, A. F.; van Leeuwen, J. M. J. *Phys. Rev. A* **1990**, *42* (10), 6052−6059.

(49) de Ruijter, M. J.; Blake, T. D.; De Coninck, J. *Langmuir* **1999**, *15*, 7836−7847.

(50) Martí, J. *J. Chem. Phys.* **1999**, *110* (14), 6876−6886.

(51) Wang, J. Y.; Betelu, S.; Law, B. M. *Phys. Rev. E* **2001**, *63*, 031601−1−031601−11.

(52) Powles, J. G.; Fowler, R. F.; Evans, W. A. B. *Phys. Lett. A* **1983**, *98* (8−9), 421−425.

(53) Mugele, F.; Becker, T.; Nokopoulos, R.; Kohonen, M.; Herminghaus, S. *J. Adhesion Sci. Technol.* **2002**, *16* (7), 951−964.

(54) Hansen, N.; Ostermeier, A. *Evolutionary Computation* **2001**, *9* (2), 159−195.

(55) Tomsic, A.; Marković, N.; Pettersson, J. B. C. *Phys. Chem. Chem. Phys.* **2001**, *3* (17), 3667−3671.

(56) Matubayasi, N.; Wakai, C.; Nakahara, M. *J. Chem. Phys.* **1997**, *107* (21), 9133−9140.